Volcanoes and ENSO: a re-appraisal with the Last Millennium Reanalysis

Feng Zhu (fzhu.la@gmail.com)
University of Southern California
Julien Emile-Geay
University of Southern California https://orcid.org/0000-0001-5920-4751
Kevin Anchukaitis
University of Arizona https://orcid.org/0000-0002-8509-8080
Gregory Hakim
University of Washington
Andrew Wittenberg
NOAA GFDL https://orcid.org/0000-0003-1680-8963
Mariano Morales
IANIGLA-CONICET
Jonathan King
University of Arizona

Article

Keywords: volcanos, El Niño-Southern Oscillation (ENSO)

Posted Date: January 8th, 2021

DOI: https://doi.org/10.21203/rs.3.rs-130239/v1

Version of Record: A version of this preprint was published at Nature Communications on February 8th, 2022. See the published version at https://doi.org/10.1038/s41467-022-28210-1.

Volcanoes and ENSO: a re-appraisal with the Last Millennium Reanalysis

Feng Zhu[1,*], Julien Emile-Geay[1], Kevin J. Anchukaitis[2,3,4], Gregory J. Hakim[5], Andrew T. Wittenberg[6], Mariano S. Morales[7,8], and Jonathan King[3,4]

[1]Department of Earth Sciences, University of Southern California, Los Angeles, CA USA
[2]Laboratory of Tree-Ring Research, University of Arizona, Tucson AZ USA
[3]School of Geography, Development, and Environment, University of Arizona, Tucson AZ USA
[4]Department of Geosciences, University of Arizona, Tucson AZ USA
[5]Department of Atmospheric Sciences, University of Washington, Seattle, WA USA
[6]NOAA Geophysical Fluid Dynamics Laboratory, Princeton, NJ, USA
[7]Instituto Argentino de Nivología, Glaciologa y Cs. Ambientales, Consejo Nacional de Investigaciones Cientficas y Técnicas (CONICET), 5500 Mendoza, Argentina
[8]Laboratorio de Dendrocronología, Universidad Continental, 12003 Huancayo, Perú
[*]Corresponding author: fengzhu@usc.edu

ABSTRACT

The potential for explosive volcanism to affect the state of the El Niño-Southern Oscillation (ENSO) has been debated since the 1980s. Several observational studies, largely based on tree rings, have since found support for a positive ENSO phase in the year following large eruptions. Models of different complexities also simulate such a response, detectable above the backdrop of internal variability – though they disagree on the underlying mechanisms. In contrast, recent coral data from the heart of the tropical Pacific suggest no uniform ENSO response to all eruptions over the last millennium. Here we leverage paleoclimate data assimilation to integrate the latest paleoclimate evidence into a consistent dynamical framework and re-appraise this relationship. Our analysis finds only a weak statistical association between volcanism and ENSO, suggestive of either no causal association, or of an insufficient number of large volcanic events over the past millennium to obtain reliable statistics. While currently available observations do not support the model-based inference that tropical eruptions promote an ENSO response, there are hints of a response to hemispherically asymmetric forcing, consistent with the "ITCZ shift" mechanism. We discuss the difficulties of conclusively establishing a volcanic influence on ENSO given the many degrees of freedom affecting the response, including eruption season, spatial characteristics of the forcing, and ENSO phase preconditioning.

Introduction

The El Niño-Southern Oscillation (ENSO), the quasi-periodic alternation of warm and cold phases of the tropical Pacific ocean-atmosphere system, is the leading source of global interannual climate variability[1]. ENSO influences weather conditions not only in the tropical Pacific[2], but also globally through atmospheric teleconnections[3]. Skillful prediction of the ENSO cycle, including its phase and amplitude, is therefore key to the successful forecasting of worldwide meteorological and oceanographic conditions at sub-seasonal to seasonal scales.

External forcing has the potential to affect ENSO variability[4]. In particular, explosive volcanism may inject large amounts of sulfate aerosols into the atmosphere, abruptly reducing incoming shortwave radiation and affecting the subsequent global ocean-atmosphere climate variability for several years[5]. A causal relationship between large eruptions and ENSO would be a significant source of climate predictability on interannual scales, and would be important for evaluating climate models' sensitivity to volcanic forcing, as well as assessing the risk of geoengineering solar radiation management schemes that emulate the stratospheric sulfate aerosol loading characteristic of large explosive eruptions[6]. The link between volcanism and ENSO has been vigorously debated since it was first proposed[7]. Since then, several tree-ring based observational studies have found support for an El Niño-like response in the year following large eruptions[8–12] and at least five mechanisms have been proposed to account for this relationship: (i) the ocean dynamical thermostat (ODT)[4,13,14], which states that the upwelled water in the eastern Pacific (EP) makes the region less sensitive to radiative forcing than the western Pacific, and leads to nonuniform Pacific SST response to uniform incoming solar radiation reductions after eruptions; (ii) the land-ocean temperature gradient (LOTG) mechanism[15–17], which states that the low thermal inertia of the land introduces a LOTG after eruptions, which affects the Pacific zonal wind anomalies and hence the ocean temperature; (iii) the subtropical wind stress curl mechanism[18,19], which states that the initial enhanced cooling in EP after eruptions leads to a negative (anticyclonic) subtropical wind stress curl,

which drives equatorward convergence of warmer subtropical waters and delays the ODT; (iv) the extratropical teleconnection mechanism[17,20], which states that volcanically induced cooling of tropical Africa weakens the West African monsoon and alters the Walker circulation; and (v) the Inter Tropical Convergence Zone (ITCZ) shift mechanism[19–22], which states that the Northern Hemisphere (NH) cooling after NH eruptions shift the ITCZ southward, which weakens the Pacific trade winds and leads to an El Niño-like response. Several studies have also suggested a La Niña-like response 2 years after an eruption[12,23], which could be due to the oscillatory nature of ENSO dynamics[12], or to the eastward position of the anomalous western North Pacific anticyclone, exciting upwelling Kelvin waves and enhancing thermocline feedback and zonal advection, leading to a greater cooling rate in the eastern Pacific[23].

Ensemble simulations with a highly simplified ENSO model[14] suggested a threshold effect that would make ENSO insensitive to all but the largest eruptions of the past millennium (approximately the magnitude of Krakatau and above). This has generally been confirmed by experiments with more realistic models[19–22,24]. However, a recent analysis of a long, monthly coral record from the heart of the tropical Pacific[25,26] suggests no uniform ENSO response to all eruptions over the last millennium, even for the largest eruptions[27]. This is in line with results from recent modeling studies using large ensembles that allow quantification of the influence of stochastic as well as deterministic elements[24]. Indeed, ENSO is thought to be affected by multiple uncertain or poorly constrained factors, including the phase of the quasi-biennial oscillation (QBO)[28], the forcing magnitude, location, and season of the eruption[19,24], as well as pre-conditioning of the ENSO state (neutral, Central Pacific El Niño, Eastern Pacific El Niño, or La Niña)[16]. Yet, observational studies on this track are hindered by the limited number of well known eruption events, the temporal resolution of volcanic forcing reconstructions, and the spatial and temporal availability of proxy records.

Paleoclimate records offer a longer period of observation but conflicting accounts: reconstructions based mostly on tree-ring proxies[8–12], which experience ENSO through teleconnections, have been used to argue of an El Niño-like response within a year of the eruption; in contrast, reconstructions using corals from the core ENSO region[26,27,29] – which provide a firsthand, albeit discontinuous, account of ENSO variations – do not support this conclusion.

In this study, we re-appraise the potential links between volcanism and ENSO, by integrating the latest paleoclimate evidence from both tree rings and corals into a consistent dynamical framework, the Last Millennium Reanalysis (LMR)[30,31], and interpret the results in the context of recent modeling work showing a large role for both initial and boundary conditions in shaping the climate response to volcanism[16,24].

Corals vs tree rings

Coral archives are a natural choice for ENSO reconstruction due to their geographical proximity to ENSO centers of action[32] and the demonstrated link between the geochemistry of their skeletons and ENSO conditions[33,34]. However, their limited time span produces discontinuous records, which can only be pieced together by splicing[26]. The longest and most complete coral ENSO record published to date[26,27,35] is located at Palmyra atoll, at the edge of the Niño 3.4 region. The record covers 535 of the past 1000 years, leaving many gaps, and with limited replication over common intervals. Tree-ring based proxies, on the other hand, have been used to build long, cross-dated, and heavily replicated reconstructions that continuously span the Common Era. Their distance to ENSO centers of action means that they rely on teleconnections between the tropical Pacific and their local terrestrial rainfall and temperature anomalies, leaving them vulnerable to confounding factors. Combining data from both archives could ameliorate their individual limitations. Before doing so, however, we compare reconstructions assimilating the two archives separately, as this provide insights into the possible causes of the discrepancy between previous studies and on how to interpret a combined signal.

Our strategy leverages the data assimilation algorithm of the Last Millennium Reanalysis (Methods). We first assimilate corals to reconstruct tropical Pacific surface temperature during the boreal winter (DJF).

Our coral collection includes the synthesis of Ocean2k[29,36], supplemented by the latest Palmyra record[27]. The resultant reconstruction is denoted as LMR (Corals), and its spatial and temporal skill is presented in Fig. 1(a,d). The skill of the Niño 3.4 reconstruction is remarkably high compared to many other existing reconstructions (see Extended Data Fig. 1), with a temporal correlation coefficient (R) of 0.86 (that is, 74% of shared variance) and a coefficient of efficiency (CE)[37] of 0.71 against ERSSTv5 (Extended Reconstructed Sea Surface Temperature v5)[38]. However, due to the temporal gaps in the Palmyra record, the reconstruction is incomplete over the last millennium (Fig. 2b) and the ensemble-mean variability collapses when Palmyra observations are unavailable.

The assimilation of tree rings for Niño 3.4 reconstruction is challenging due to their distance to the target region. To overcome this, we gather the six best tree-ring based Niño 3.4 predictors identified by Li et al.[10] (denoted as Li13b6): the first two principal components of the North American Drought Atlas (NADA) (Version 2a)[39] and Monsoon Asia Drought Atlas (MADA)[40], the Kauri tree-ring composite[41], and the South America Altiplano tree-ring composite[42] (Extended Data Fig. 2), and assimilate them in LMR as proxies for Niño 3.4 SST (see Methods). The resultant reconstruction, denoted as LMR (Li13b6) in Fig. 1b,e displays skill comparable to LMR (Corals), though slightly weaker, with $R = 0.75$ and $CE = 0.57$. Note

that the scatter plots in Extended Data Fig. 2 (m-r) indicate that Li13b6 predictors tend to underestimate the Niño 3.4 anomaly in year 1 after instrumental era eruptions (as the colored dots tend to hover above the linear model fit), yet this behavior is not obvious in the reconstruction LMR (Li13b6) (Fig. 1h), suggesting an advantage for processing the proxy observations within the LMR paleo-data assimilation framework. The spatial verification (Fig. 1b) indicates that the reconstruction skill peaks around the center of the Niño 3.4 region and decays quickly away from it. A major advantage of the tree-based reconstruction is its continuous nature over the past millennium (Fig. 2c).

We next assess the ENSO response to volcanism in both reconstructions. To perform an equitable comparison, we select large eruptions defined as volcanic stratospheric sulfur injection (VSSI) greater than 6 Tg S according to the eVolv2k version 3 dataset[43], and focus on periods when the Palmyra coral record is available (Fig. 2a). We assess the forced ENSO responses using both the widely-used superposed epoch analysis (SEA) approach (also known as compositing), as well as a ranking analysis (see Methods). The SEA (Fig. 3a,b) applied to the 12 large events when Palmyra is available (Fig. 2a) suggests that there is no Niño 3.4 composite value that is significantly higher than that of randomly drawn non-volcanic years, even at the relatively permissive 90% level.

However, SEA is sensitive to dating uncertainties, as the compositing procedure requires that the reconstruction segments of individual events align precisely, without which otherwise minor timing offsets can compound and damp the composite signal. SEA may also be affected by the small sample size. This may first come into play through a type I error, which is tested in the SI Text 2. We find that even small ensembles ($n = 5$) can mitigate this problem, so it is not material for this particular issue. However, like all averaging methods, an SEA carried over a small sample may be dominated by a small number of events with extreme anomalies, with most events showing a modest response[44]. Thus, a "significant" composite response is a necessary but insufficient condition to establish a physical response. Only when most of the events show strong responses can we be confident about the robustness of the relationship. Therefore, it is important to parse composites into the contributions from, and consistency of, individual events. This is achieved through a ranking analysis (Fig. 3c-f), which compares the Niño 3.4 response of each event to the distribution of all non-volcanic years. Events with response values larger than a certain quantile (say, 80, 90, or 95%) of the distribution of non-volcanic years are considered "significant".

Though the ranks of eruption-year events in the two reconstructions do not agree with each other in detail, both LMR (Corals) and LMR (Li13b6) point to the same conclusion: that most eruption years are not statistically different from non-eruption years in both year 0 and year 1, at any significance level.

Combining corals and tree rings

Given this agreement, we combine both archives to perform a continuous reconstruction, denoted as LMR (Corals+Li13b6). Verification statistics (Fig. 1c,f) show a slight skill improvement compared to LMR (Corals), with $R = 0.86$ and $CE = 0.71$ against ERSSTv5. More importantly, the temporal gaps in LMR (Corals) over the past millennium are now filled with the information from Li13b6 (Fig. 2), which allows a larger sample size of eruption events, hence a more robust evaluation of ENSO's response to volcanism.

The SEA on LMR (Corals+Li13b6) suggests once again that there is no significant post eruption Niño 3.4 composite response (Fig. 4a,b) whether using the previously selected 12 events, or all 22 large eruptions of the last millennium (Fig. 2a). Similarly, the ranking analysis (Fig. 4c-f) indicates low significance ratio in year 0 and year 1 for both cases of selected events.

Overall, both SEA and ranking analysis support the conclusion that the statistical link between ENSO phases and last millennium volcanism is weak. It is worth noting that, comparing rankings in the case of 12 (Fig. 4c,e) vs. 22 events (Fig. 4d,f), events after 1850 CE appear to be significant more likely, suggesting that the sensitivity is time-dependent, a possibility that we investigate below.

A non-stationary sensitivity?

While our results appear to reconcile previous results obtained from corals and tree rings, discrepancies remain in the published literature (e.g. Dee et al.[27], hereafter D20, vs Li et al.[10], hereafter Li13).

An important factor in such comparisons is the choice of events used to diagnose the volcanic signal. Due to the temporal coverage of the Palmyra coral record, D20 performed SEA mainly on early eruptions (1171, 1230, 1258, 1458, 1641, 1695 CE), while Li13 performed SEA on a pool with more recent eruptions (1350, 1360, 1450, 1580, 1586, 1593, 1600, 1641, 1660, 1673, 1680, 1815, 1822, 1831, 1835, 1883, 1902, 1913, 1951, 1963, 1982, 1991 CE). Extended Data Fig. 3a indicates that the Li13 reconstruction is heavily heteroskedastic: the variance is less than 1 over much of the pre-instrumental period (before 1850 CE), and larger after that point. If post 1850 CE events are excluded, the significance level of the year 1 response drops from >99% to around 90% (Extended Data Fig. 3b, dashed dotted curve). This alone suggests that instrumental-era events are dominating the SEA, leading to a biased result.

To assess individual events, we compare rankings using all eruptions vs pre-instrumental eruptions only (Extended Data Fig. 3c,d). It can be seen that the instrumental period eruptions overall show a stronger Niño 3.4 anomaly than the pre-instrumental period eruptions (Extended Data Fig. 3c). Without instrumental-era eruptions, only (3, 2, 1) out of 15 events show a larger Niño 3.4 response than (80%, 90%, 95%) of the non-volcanic years (Extended Data Fig. 3d), indicating that most of the pre-instrumental period eruptions are not significantly different from non-volcanic years.

The above analysis suggests that the reconstructed ENSO response to volcanism is non-stationary, at least between pre-instrumental and instrumental period eruptions.

This could be caused by data attrition, which reduces variability of a reconstruction going back in time since the proxy observations provide the only source of variability in our reconstructions. Moreover, MADA is compiled using a correlation-weighted, ensemble-based modification of the "point-by-point regression"[40], and the ensemble members become less similar to each other during earlier periods, over which temporal variability is damped compared to recent intervals. In addition, dating accuracy is a non-negligible problem for fossil corals[45], where errors compound back in time, potentially reducing the variability of composite series derived from them[34]. In addition, we note that the instrumental period is quite short and devoid of the very large eruptions that occur in the pre-instrumental period, so results obtained over this period may not be statistically representative. Furthermore, instrumental records have shown evidence of the potential of coincidence between ENSO activity and volcanism, at least for the Agung (1963), El Chichon (1982), and Pinatubo (1991) eruptions, when strong El Niño events were already underway before the eruptions went off[46].

Repeating the above analysis in Extended Data Fig. 3 on LMR (Li13b6) and LMR (Corals+Li13b6), we see similar characteristics (SI Fig. 5 & 6) to that of Li13, suggesting that the seemingly divergent conclusions between Li13 and our study, regarding the statistical significance of ENSO response to volcanism, are mainly caused by different choices of eruption key dates (see SI Text 3 for details).

Effects of forcing asymmetry

Previous studies have suggested that the hemispheric asymmetry of volcanic forcing is another factor that may differentially affect ENSO activity[15,20,21,24]. Therefore, we investigate the relationship between forcing parameters and the Niño 3.4 SST from LMR (Corals+Li13b6). Tropical eruption events are categorized by different hemispheric asymmetry levels (below 0.8, between 0.8 and 1.5, and above 1.5) defined as aerosol spread based on ratio of Greenland to Antarctic sulfate flux[43]. Extreme events are defined as having a VSSI>20 (1230, 1257, 1458, 1815). Extended Data Fig. 4 indicates a consistently positive linear relationship between VSSI and year 0 Niño 3.4 responses for events with hemispheric asymmetry larger than 1.5, and between 0.8 and 1.5, although the latter category is dominated by the 1257 extreme event. The relationship for year 1 Niño 3.4 responses is weak for both categories, and there are not enough events to get any meaningful insights for events with asymmetry smaller than 0.8, nor with extreme events. The positive linear relationship between VSSI and year 0 Niño 3.4 response for strongly asymmetric tropical eruptions is in agreement with the ITCZ shift mechanism[19–22]. However, the relatively small sample size invites caution about the interpretation. Potentially confounding factors are discussed below.

Discussion

Using state-of-the-art datasets and methods, combining the strengths of both coral and tree-ring records, the present evidence is as yet unable to detect an effect of explosive volcanism on ENSO phase, consistent with D20[27]. This conclusion is supported by corals and trees independently. Yet, corals and trees disagree regarding the relative rank between individual events (Fig. 3). This issue might be caused by attrition in both networks, which reduces reconstruction variance back in time. Similarly, temporal gaps in the Palmyra coral record limit the pool of eruption events and non-volcanic years to a smaller size, making the comparison less stable.

Beyond the issue of attrition, proxy archives harbor limitations of their own. The tree-ring records used here, for instance, are sensitive to the local hydrological expression of volcanic eruptions, which may be mistaken for the remote effects of ENSO via teleconnections[22]. The ENSO reconstruction based on the South American Altiplano composite[42] also suggests that the non-stationary behavior of ENSO variance is masked by intrinsic tree-ring width variability. Indeed, when ENSO variance is low, the teleconnection is weak, and tree ring variability is more reflective of local temperature and moisture conditions than those from the remote tropical Pacific; such non-stationarity may obscure the volcanoes-ENSO link. The current coral network is more proximal to ENSO centers of action, yet is dominated by records from the western and central equatorial Pacific (Fig. 1a) which capture La Niña events more faithfully than El Niño events, and tend to underestimate the amplitude of large eastern Pacific (EP) events[34,47]. The sparse geographical coverage is another issue, preventing the estimation of tropics-wide SST in a way that would allow for a robust calculation of relative sea surface temperature (RSST)[17]. Indeed, it has been suggested that El Niño phases could be enhanced by volcanism even when the absolute SST signal in the central and eastern tropical Pacific is weak[48].

RSST highlights the impact of volcanism on ENSO relative to the tropical mean cooling, and is computable in our reconstructed SST fields. This is shown in Extended Data Fig. 5, which displays a temporally-flat tropical average temperature anomaly for most of the years between 1100-2000 CE, resulting in RSST-based Niño 3.4 anomalies that are indistinguishable from the SST-based ones. This is a direct result of the sparse coral network before the nineteenth century, and will not improve until this network is vastly expanded over tropical oceans. However, even with the RSST conversion, we still observe consistently low significance ratio in the ranking analysis of the last millennium climate model simulations (see SI Text S4 for details).

Another caveat comes from limitations associated with the choice of the model prior in the LMR paleo-DA framework. The model prior here refers to the model simulation from which climate states are chosen at random by the Kalman filter algorithm. Its chief role is to provide the spatial covariance information within and between fields, and affects how the information from proxy observations propagates to locations where those observations are not available. According to a recent study[49], the known biases in the location of the South Pacific Convergence Zone (SPCZ) in most climate models leads to incorrect inferences about Niño 3.4 SST from corals located in the SPCZ region, in such a paleoclimate data assimilation context. Moreover, ref. 49 shows that corals located in both the SPCZ and Niño 3.4 regions produce local cooling during the 1809 and 1815 eruptions, but all prior ensembles considered (including those drawn from 20th century reanalyses) have a covariance pattern that yields remote influence (that is, the influence of one region on another) inconsistent with this pattern. In addition to model bias, this suggests that model priors conditional on eruption time would be important for properly representing the information in proxy records. We note that, in the present study, these biases are mitigated prior to 1800, when only proxies tied to the Niño 3.4 index are used.

Finally, a recent modeling study[24] suggests that the ENSO response to volcanism is rather weak during DJF because it changes sign around that season. Yet, the response could be strong before the sign changes, which is usually during January-September (JAS) and/or October-December (OND). Repeating our analysis using JAS and OND as target seasons, we find our conclusions insensitive to this choice (SI Text 5). This is in apparent contradiction to that modeling study[24], yet may be explained by the limitations of currently available proxy records noted above. Assigning eruption events to specific years based on volcanic forcing reconstructions could also lead to time offsets in analyses using different target seasons[50], which will potentially obscure the relation to eruption events. This is a problem that we cannot resolve currently without a better knowledge of the eruption season.

That we do not find a consistent ENSO response in the relatively small statistical sample of the last millennium is not evidence that there is zero predictability associated with volcanoes. As suggested by recent modeling studies[16,24], the forcing magnitude, location, and season of the eruption, as well as pre-conditioning of the ENSO state can greatly affect the ENSO response to volcanic eruptions. These multiple factors must align to favor the development of ENSO events, providing a source of predictability only when these factors are known with a sufficient degree of accuracy. It is therefore reasonable to expect that the lack of an observed, consistent relationship between ENSO phases and explosive volcanism in our reconstructions may be due, in part, to an imperfect knowledge of these factors. However, even when controlling for eruption timing in PMIP3 and CESM-LME simulations, a ranking analysis still demonstrates an inconsistent ENSO response to volcanism when this major source of variability is held fixed (SI Text 4), suggesting that all factors need to be jointly determined, or that a larger ensemble is needed to discern common trends.

Given the large number of degrees of freedom, a large sample size is needed to isolate a consistent signal – larger perhaps than offered by the past millennium. It is thus important to develop more high-resolution proxy records spanning the tropical oceans over the last millennium, and possibly extend them through the longer Holocene. The reconstruction of volcanic forcing also needs to be expanded with longer temporal coverage for more robust statistics. Until these goals have been achieved, it is unclear how much one can conclude from the paleoclimate record about the contribution of volcanic eruptions to ENSO dynamics, or to the assessment of the risks posed by solar radiation management strategies in relation to ENSO.

References

1. Sarachik, E. S. & Cane, M. A. *The El Niño-Southern Oscillation Phenomenon* (Cambridge University Press, Cambridge, UK, 2010).
2. McPhaden, M. J., Lee, T. & McClurg, D. El Niño and its relationship to changing background conditions in the tropical Pacific Ocean. *Geophys. Res. Lett.* **38**, DOI: 10.1029/2011GL048275 (2011).
3. Diaz, H. F., Hoerling, M. P. & Eischeid, J. K. ENSO variability, teleconnections and climate change. *Int. J. Climatol.* **21**, 1845–1862, DOI: 10.1002/joc.631 (2001).
4. Mann, M. E., Cane, M. A., Zebiak, S. E. & Clement, A. Volcanic and Solar Forcing of the Tropical Pacific over the Past 1000 Years. *J. Clim.* **18**, 447–456, DOI: 10.1175/JCLI-3276.1 (2005).
5. Robock, A. Volcanic eruptions and climate. *Rev. Geophys.* **38**, 191–220, DOI: 10.1029/1998RG000054 (2000).

6. Robock, A., Marquardt, A., Kravitz, B. & Stenchikov, G. Benefits, risks, and costs of stratospheric geoengineering. *Geophys. Res. Lett.* **36**, DOI: 10.1029/2009GL039209 (2009).

7. Handler, P. Possible association of stratospheric aerosols and El Niño type events. *Geophys. Res. Lett.* **11**, 1121–1124, DOI: 10.1029/GL011i011p01121 (1984).

8. Adams, J., Mann, M. E. & Ammann, C. M. Proxy evidence for an El Niño-like response to volcanic forcing. *Nature* **426**, 274–278, DOI: 10.1038/nature02101 (2003).

9. McGregor, S., Timmermann, A. & Timm, O. A unified proxy for ENSO and PDO variability since 1650. *Clim. Past* **6**, 1–17, DOI: https://doi.org/10.5194/cp-6-1-2010 (2010). Publisher: Copernicus GmbH.

10. Li, J. *et al.* El Niño modulations over the past seven centuries. *Nat. Clim. Chang.* **3**, 822–826, DOI: 10.1038/nclimate1936 (2013).

11. Wahl, E. R., Diaz, H. F., Smerdon, J. E. & Ammann, C. M. Late winter temperature response to large tropical volcanic eruptions in temperate western North America: Relationship to ENSO phases. *Glob. Planet. Chang.* **122**, 238–250, DOI: 10.1016/j.gloplacha.2014.08.005 (2014).

12. McGregor, S. *et al. The Effect of Strong Volcanic Eruptions on ENSO*, chap. 12, 267–287 (American Geophysical Union (AGU), 2020). DOI: 10.1002/9781119548164.ch12.

13. Clement, A. C., Seager, R., Cane, M. A. & Zebiak, S. E. An Ocean Dynamical Thermostat. *J. Clim.* **9**, 2190–2196, DOI: 10.1175/1520-0442(1996)009<2190:AODT>2.0.CO;2 (1996).

14. Emile-Geay, J., Seager, R., Cane, M. A., Cook, E. R. & Haug, G. H. Volcanoes and ENSO over the Past Millennium. *J. Clim.* **21**, 3134–3148, DOI: 10.1175/2007JCLI1884.1 (2008).

15. Ohba, M., Shiogama, H., Yokohata, T. & Watanabe, M. Impact of Strong Tropical Volcanic Eruptions on ENSO Simulated in a Coupled GCM. *J. Clim.* **26**, 5169–5182, DOI: 10.1175/JCLI-D-12-00471.1 (2013). Publisher: American Meteorological Society.

16. Predybaylo, E., Stenchikov, G. L., Wittenberg, A. T. & Zeng, F. Impacts of a Pinatubo-size volcanic eruption on ENSO. *J. Geophys. Res. Atmospheres* **122**, 925–947, DOI: 10.1002/2016JD025796 (2017). _eprint: https://agupubs.onlinelibrary.wiley.com/doi/pdf/10.1002/2016JD025796.

17. Khodri, M. *et al.* Tropical explosive volcanic eruptions can trigger El Niño by cooling tropical Africa. *Nat. Commun.* **8**, 1–13, DOI: 10.1038/s41467-017-00755-6 (2017). Number: 1 Publisher: Nature Publishing Group.

18. McGregor, S. & Timmermann, A. The Effect of Explosive Tropical Volcanism on ENSO. *J. Clim.* **24**, 2178–2191, DOI: 10.1175/2010JCLI3990.1 (2011). Publisher: American Meteorological Society.

19. Stevenson, S., Fasullo, J. T., Otto-Bliesner, B. L., Tomas, R. A. & Gao, C. Role of eruption season in reconciling model and proxy responses to tropical volcanism. *Proc. Natl. Acad. Sci.* **114**, 1822–1826, DOI: 10.1073/pnas.1612505114 (2017).

20. Pausata, F. S. R., Zanchettin, D., Karamperidou, C., Caballero, R. & Battisti, D. S. ITCZ shift and extratropical teleconnections drive ENSO response to volcanic eruptions. *Sci. Adv.* **6**, eaaz5006, DOI: 10.1126/sciadv.aaz5006 (2020). Publisher: American Association for the Advancement of Science Section: Research Article.

21. Pausata, F. S. R., Chafik, L., Caballero, R. & Battisti, D. S. Impacts of high-latitude volcanic eruptions on ENSO and AMOC. *Proc. Natl. Acad. Sci.* **112**, 13784–13788, DOI: 10.1073/pnas.1509153112 (2015).

22. Stevenson, S., Otto-Bliesner, B., Fasullo, J. & Brady, E. El Niño Like Hydroclimate Responses to Last Millennium Volcanic Eruptions. *J. Clim.* **29**, 2907–2921, DOI: 10.1175/JCLI-D-15-0239.1 (2016).

23. Sun, W. *et al.* A "La Niña-like" state occurring in the second year after large tropical volcanic eruptions during the past 1500 years. *Clim. Dyn.* **52**, 7495–7509, DOI: 10.1007/s00382-018-4163-x (2019).

24. Predybaylo, E., Stenchikov, G., Wittenberg, A. T. & Osipov, S. El Niño/Southern Oscillation response to low-latitude volcanic eruptions depends on ocean pre-conditions and eruption timing. *Commun. Earth & Environ.* **1**, 1–13, DOI: 10.1038/s43247-020-0013-y (2020). Number: 1 Publisher: Nature Publishing Group.

25. Cobb, K. M., Charles, C. D. & Hunter, D. E. A central tropical Pacific coral demonstrates Pacific, Indian, and Atlantic decadal climate connections. *Geophys. Res. Lett.* **28**, 2209–2212, DOI: 10.1029/2001GL012919 (2001).

26. Cobb, K. M., Charles, C. D., Cheng, H. & Edwards, R. L. El Niño/Southern Oscillation and tropical Pacific climate during the last millennium. *Nature* **424**, 271, DOI: 10.1038/nature01779 (2003).

27. Dee, S. G. *et al.* No consistent ENSO response to volcanic forcing over the last millennium. *Science* **367**, 1477–1481, DOI: 10.1126/science.aax2000 (2020). Publisher: American Association for the Advancement of Science Section: Report.

28. Taguchi, M. Observed connection of the stratospheric quasi-biennial oscillation with El NiñoSouthern Oscillation in radiosonde data. *J. Geophys. Res. Atmospheres* **115**, DOI: 10.1029/2010JD014325 (2010). _eprint: https://agupubs.onlinelibrary.wiley.com/doi/pdf/10.1029/2010JD014325.

29. Tierney, J. E. *et al.* Tropical sea surface temperatures for the past four centuries reconstructed from coral archives. *Paleoceanography* **30**, 226–252, DOI: 10.1002/2014PA002717 (2015). _eprint: https://agupubs.onlinelibrary.wiley.com/doi/pdf/10.1002/2014PA002717.

30. Hakim, G. J. *et al.* The last millennium climate reanalysis project: Framework and first results. *J. Geophys. Res. Atmospheres* **121**, 2016JD024751, DOI: 10.1002/2016JD024751 (2016).

31. Tardif, R. *et al.* Last Millennium Reanalysis with an expanded proxy database and seasonal proxy modeling. *Clim. Past* **15**, 1251–1273, DOI: https://doi.org/10.5194/cp-15-1251-2019 (2019).

32. Wilson, R. *et al.* Reconstructing ENSO: the influence of method, proxy data, climate forcing and teleconnections. *J. Quat. Sci.* **25**, 62–78, DOI: 10.1002/jqs.1297 (2010).

33. Lough, J. M. Climate records from corals. *Wiley Interdiscip. Rev. Clim. Chang.* **1**, 318–331, DOI: 10.1002/wcc.39 (2010).

34. Emile-Geay, J., Cobb, K. M., Cole, J. E., Elliot, M. & Zhu, F. *Past ENSO Variability*, chap. 5, 87–118 (American Geophysical Union (AGU), 2020). DOI: 10.1002/9781119548164.ch5.

35. Cobb, K. M. *et al.* Highly Variable El Niño-Southern Oscillation Throughout the Holocene. *Science* **339**, 67–70, DOI: 10.1126/science.1228246 (2013). Publisher: American Association for the Advancement of Science Section: Report.

36. PAGES2k Consortium. A global multiproxy database for temperature reconstructions of the Common Era. *Sci. Data* **4**, 170088, DOI: 10.1038/sdata.2017.88 (2017).

37. Nash, J. & Sutcliffe, J. River flow forecasting through conceptual models part I – A discussion of principles. *J. Hydrol.* **10**, 282–290, DOI: 10.1016/0022-1694(70)90255-6 (1970).

38. Huang, B. *et al.* Extended Reconstructed Sea Surface Temperature, Version 5 (ERSSTv5): Upgrades, Validations, and Intercomparisons. *J. Clim.* **30**, 8179–8205, DOI: 10.1175/JCLI-D-16-0836.1 (2017). Publisher: American Meteorological Society.

39. Cook, E. R., Woodhouse, C. A., Eakin, C. M., Meko, D. M. & Stahle, D. W. Long-Term Aridity Changes in the Western United States. *Science* **306**, 1015–1018, DOI: 10.1126/science.1102586 (2004).

40. Cook, E. R. *et al.* Asian Monsoon Failure and Megadrought During the Last Millennium. *Science* **328**, 486–489, DOI: 10.1126/science.1185188 (2010). Publisher: American Association for the Advancement of Science Section: Report.

41. Fowler, A. M., Boswijk, G., Gergis, J. & Lorrey, A. ENSO history recorded in Agathis australis (kauri) tree rings. Part A: kauri's potential as an ENSO proxy. *Int. J. Climatol.* **28**, 1–20, DOI: 10.1002/joc.1525 (2008). _eprint: https://rmets.onlinelibrary.wiley.com/doi/pdf/10.1002/joc.1525.

42. Morales, M. S. *et al.* Precipitation changes in the South American Altiplano since 1300 AD reconstructed by tree-rings. *Clim. Past* **8**, 653–666, DOI: https://doi.org/10.5194/cp-8-653-2012 (2012). Publisher: Copernicus GmbH.

43. Toohey, M. & Sigl, M. Volcanic stratospheric sulfur injections and aerosol optical depth from 500 BCE to 1900 CE. *Earth Syst. Sci. Data* **9**, 809–831, DOI: https://doi.org/10.5194/essd-9-809-2017 (2017).

44. Rao, M. P. *et al.* A double bootstrap approach to Superposed Epoch Analysis to evaluate response uncertainty. *Dendrochronologia* **55**, 119–124, DOI: 10.1016/j.dendro.2019.05.001 (2019).

45. Comboul, M. *et al.* A probabilistic model of chronological errors in layer-counted climate proxies: applications to annually banded coral archives. *Clim. Past* **10**, 825–841, DOI: https://doi.org/10.5194/cp-10-825-2014 (2014).

46. Lehner, F., Schurer, A. P., Hegerl, G. C., Deser, C. & Frölicher, T. L. The importance of ENSO phase during volcanic eruptions for detection and attribution. *Geophys. Res. Lett.* **43**, 2851–2858, DOI: https://doi.org/10.1002/2016GL067935 (2016). _eprint: https://agupubs.onlinelibrary.wiley.com/doi/pdf/10.1002/2016GL067935.

47. Emile-Geay, J., Cobb, K. M., Mann, M. E. & Wittenberg, A. T. Estimating Central Equatorial Pacific SST Variability over the Past Millennium. Part II: Reconstructions and Implications. *J. Clim.* **26**, 2329–2352, DOI: 10.1175/JCLI-D-11-00511.1 (2013). Publisher: American Meteorological Society.

48. Robock, A. Comment on No consistent ENSO response to volcanic forcing over the last millennium. *Science* **369**, DOI: 10.1126/science.abc0502 (2020). Publisher: American Association for the Advancement of Science Section: Technical Comments.

49. Sanchez, S. C., Hakim, G. J. & Saenger, C. P. Climate model teleconnection patterns govern the Niño 3.4 response to early 19th century volcanism in coral-based data assimilation reconstructions. *J. Clim.* 1–51, DOI: 10.1175/JCLI-D-20-0549.1 (2020).

50. Anchukaitis, K. J. *et al.* Influence of volcanic eruptions on the climate of the Asian monsoon region. *Geophys. Res. Lett.* **37**, DOI: 10.1029/2010GL044843 (2010). _eprint: https://agupubs.onlinelibrary.wiley.com/doi/pdf/10.1029/2010GL044843.

Methods

The Last Millennium Reanalysis data assimilation framework

The version of the Last Millennium Reanalysis (LMR) data assimilation (DA) framework used here[30,31] is an offline ensemble Kalman filter[51], optimized for multivariate climate field reconstruction[52]. It consists of a collection of prior states generated by the CCSM4 climate model, a proxy database, a set of "forward operators" or proxy system models (PSMs)[53] that translates the environmental variables to the proxy space, and an ensemble Kalman filter operator. In our implementation, the temporal variation of the posterior stems entirely from the temporal information from the proxies, while the covariance structure of the model prior serves to spread the temporal information of each proxy to remote regions and other variables than those directly related to the proxy. For further details, see studies[30,31]. For computational convenience, this study utilizes a fast implementation of the LMR framework, LMRt[54]. In each assimilation experiment, we perform 50 Monte Carlo iterations, each using a different randomly chosen 100-member ensemble states from the CCSM4 last millennium simulation[55] as the model prior. No proxy randomization is performed to guarantee the similarity between each ensemble member so that the median curve of the reconstructed Niño 3.4 index series is representative of the whole reconstruction product. The default covariance localization[56] radius of 25,000 km is applied, and we note that the results are insensitive to this exact choice.

Note that the calibration period for the PSMs is 1850-2000 CE so as to achieve the best reconstruction skill. To guard against potential overfitting, as well as the potential impact of climate change we see in NADA PC2 and the Kauri composite (Extended Data Fig. 2d,e), a cross-validation of the reconstructed Niño 3.4 is performed with disjoint calibration and validation periods (see SI Text 1); the result suggests that the reconstruction skill is stable to this choice.

Data Sources

We consider information from seasonally-sensitive or monthly-resolved proxy records. Coral records are from the Ocean2k compilation[29] updated with the latest Palmyra data[27]. Each coral record is treated as a proxy for local sea surface temperature (SST), and is calibrated over 1850-2000 CE through a univariate linear regression procedure against the local, boreal winter (DJF) SST, which shows high reconstruction skill as in previous studies[30,31]. Experiments with a model that takes the oxygen isotopic composition of seawater into account did not produce noticeable improvements, which is in agreement with a recent study[49].Tree-based records from both hemispheres are taken from a previous reconstruction (Li13[10]), using seven predictor timeseries. The six best predictors are the first two principal components (PCs) of North American Drought Atlas (NADA) (Version 2a)[39] and Monsoon Asia Drought Atlas (MADA)[40], the Kauri tree-ring composite[41], as well as the South American Altiplano composite[42], with the explained variance of Li13 being 11.2%, 8.4%, 40.5%, 24.2%, 38.1%, 56.5%, respectively. The other predictor is the west-central Argentina composite[57], which contributes negligibly to reconstruction skill (with an explained variance of Li13 of 1.8%), and is ignored here. We refer to these best six records as "Li13b6".

We reproduced the principal components of NADA and MADA via principal component analysis (PCA)[58], so that we are able to extend the timespan of NADA PCs to 1001-2000 CE, compared to the original timespan (1300-2000 CE) in Li13. The timespan of the reproduced MADA PCs remains 1300-2000 CE due to the temporal coverage of MADA itself[40]. The Kauri tree-ring composite covers the 1578-2003 period, and the South American Altiplano tree-ring composite covers 1290-2010 CE. Data beyond 2000 CE are not used since our reconstruction stops at 2000 CE. Note that the South American Altiplano composite we use is the residual chronology instead of the standard chronology. A residual chronology is obtained by filtering (prewhitening) the standard chronology via autoregressive modeling[59]. This procedure removes some low-frequency variability and therefore emphasizes the higher-frequency variability in tree-ring growth and remains appropriate for the reconstruction of interannual variability. All six predictors are treated as proxies for Niño3.4 SST and are calibrated over 1850-2000 CE through a univariate linear regression procedure against the Niño3.4 index series derived from a spatially completed version of HadCRUT4.6[60] leveraging the GraphEM[61] algorithm. Extended Data Fig. 2g-k show a temporal verification of each predictor against the Niño 3.4 series derived from ERSSTv5 as in Fig. 1d-f.

Superposed epoch analysis

The superposed epoch analysis (SEA)[62] is a widely-used method for analyzing the climate responses to volcanic eruptions[10,27,63]. In our case, we extract the median Niño3.4 index series as the target for analysis for each LMR reconstruction. Large eruption events are defined as a volcanic stratospheric sulfur injection (VSSI) greater than 6 Tg S according to the eVolv2k version 3 dataset[43]. SEA considers segments around each event , here extending from 3 years prior to the event year and 6 years after the event year. As in previous work[27], the mean of the 3 years prior to the event year is removed so that each segment represents the anomaly response relative to the mean state before each event. A composite is obtained by averaging these 10-year windows. A bootstrap significance test is then performed: the same number of years as the eruption events under consideration are randomly drawn from the pool of non-volcanic years for 1000 times, and the composite is calculated for each draw with an identical process that we calculate the composite for eruption years, based on which we calculate the 1%, 5%, 10%, 90%, 95%, and 99% quantiles of the non-volcanic years at each relative year as the significance levels. Here the non-volcanic years are defined as the years excluding eruption events defined as VSSI>1.

Ranking analysis

A ranking analysis[64] is designed to assess whether the ENSO response to each individual event is significantly different from non-volcanic years. Similar to SEA, we extract the median Niño 3.4 index series from each LMR reconstruction as the target for analysis, and collect the segments around each eruption event, with a window from 3 years prior to the event year and 6 years after the event year, and the mean of the 3 years prior to each event year is removed. Then we decide the relative year we would like to evaluate (year 0 and year 1 in this study), and a list of Niño 3.4 anomaly values for each event is formed, which we sort in ascending order. We collect the Niño 3.4 anomaly values for all non-volcanic years and perform a kernel density estimation with a Gaussian kernel with a bandwidth selected by Scott's Rule[65], after which its 50%, 80%, 90%, and 95% quantiles are calculated. Events with response values larger than the 80%, 90%, and 95% quantiles are considered "significant" at each level, and a significance ratio is calculated. For instance, a significance ratio $(a,b,c)/n$ means that (a,b,c) out of n events have response values higher than the (80%, 90%, 95%) quantiles of the distribution of non-volcanic years.

Methods-only References

51. Evensen, G. *Data Assimilation: The Ensemble Kalman Filter* (Springer, 2009), 2nd ed. 2009 edition edn.

52. Steiger, N. J., Hakim, G. J., Steig, E. J., Battisti, D. S. & Roe, G. H. Assimilation of Time-Averaged Pseudoproxies for Climate Reconstruction. *J. Clim.* **27**, 426–441, DOI: 10.1175/JCLI-D-12-00693.1 (2013).

53. Evans, M. N., Tolwinski-Ward, S. E., Thompson, D. M. & Anchukaitis, K. J. Applications of proxy system modeling in high resolution paleoclimatology. *Quat. Sci. Rev.* **76**, 16–28, DOI: 10.1016/j.quascirev.2013.05.024 (2013).

54. Zhu, F., Emile-Geay, J., Hakim, G. J., Tardif, R. & Perkins, A. LMR Turbo (LMRt): a lightweight implementation of the LMR framework, DOI: 10.5281/zenodo.3590258 (2019).

55. Landrum, L. *et al.* Last Millennium Climate and Its Variability in CCSM4. *J. Clim.* **26**, 1085–1111, DOI: 10.1175/JCLI-D-11-00326.1 (2012).

56. Gaspari, G. & Cohn, S. E. Construction of correlation functions in two and three dimensions. *Q. J. Royal Meteorol. Soc.* **125**, 723–757, DOI: 10.1002/qj.49712555417 (1999). _eprint: https://rmets.onlinelibrary.wiley.com/doi/pdf/10.1002/qj.49712555417.

57. Villalba, R. *et al.* Interdecadal climatic variations in millennial temperature reconstructions from southern South America. In Jones, P. D., Bradley, R. S. & Jouzel, J. (eds.) *Climatic Variations and Forcing Mechanisms of the Last 2000 Years*, NATO ASI Series, 161–189, DOI: 10.1007/978-3-642-61113-1_9 (Springer, Berlin, Heidelberg, 1996).

58. Pearson, K. On lines and planes of closest fit to systems of points in space. *The London, Edinburgh, Dublin Philos. Mag. J. Sci.* **2**, 559–572, DOI: 10.1080/14786440109462720 (1901). Publisher: Taylor & Francis _eprint: https://doi.org/10.1080/14786440109462720.

59. Cook, E. R. & Kairiukstis, L. A. (eds.) *Methods of Dendrochronology: Applications in the Environmental Sciences* (Springer Netherlands, 1990).

60. Vaccaro, A. *et al.* Climate field completion via markov random fields - application to the hadcrut4.6 temperature dataset. *J. Clim.* (revised).

61. Guillot, D., Rajaratnam, B. & Emile-Geay, J. Statistical paleoclimate reconstructions via Markov random fields. *The Annals Appl. Stat.* **9**, 324–352, DOI: 10.1214/14-AOAS794 (2015).

62. Haurwitz, M. W. & Brier, G. W. A Critique of the Superposed Epoch Analysis Method: Its Application to SolarWeather Relations. *Mon. Weather. Rev.* **109**, 2074–2079, DOI: 10.1175/1520-0493(1981)109<2074:ACOTSE>2.0.CO;2 (1981).

63. Zhu, F., Emile-Geay, J., Hakim, G. J., King, J. & Anchukaitis, K. J. Resolving the Differences in the Simulated and Reconstructed Temperature Response to Volcanism. *Geophys. Res. Lett.* **47**, e2019GL086908, DOI: 10.1029/2019GL086908 (2020). _eprint: https://agupubs.onlinelibrary.wiley.com/doi/pdf/10.1029/2019GL086908.

64. Guillet, S. *et al.* Climate response to the Samalas volcanic eruption in 1257 revealed by proxy records. *Nat. Geosci.* **10**, 123–128, DOI: 10.1038/ngeo2875 (2017).

65. Scott, D. W. *Multivariate Density Estimation: Theory, Practice, and Visualization* (Wiley, New York, 1992), 1st edition edn.

66. Bunge, L. & Clarke, A. J. A Verified Estimation of the El Niño Index Niño-3.4 since 1877. *J. Clim.* **22**, 3979–3992, DOI: 10.1175/2009JCLI2724.1 (2009).

67. Steiger, N. J., Smerdon, J. E., Cook, E. R. & Cook, B. I. A reconstruction of global hydroclimate and dynamical variables over the Common Era. *Sci. Data* **5**, 1–15, DOI: 10.1038/sdata.2018.86 (2018).

Acknowledgements

The authors acknowledge support from the Climate Program Office of the National Oceanographic and Atmospheric Administration (grants NA18OAR4310426 to USC, NA18OAR4310422 to UW, and NA18OAR4310420 to UA) GJH also acknowledges support from the NSF through grant AGS–1702423.

Author contributions statement

JEG, KJA, GJH, ATW, and FZ designed the research. FZ conducted all calculations and produced all the figures. All authors interpreted results and wrote the paper.

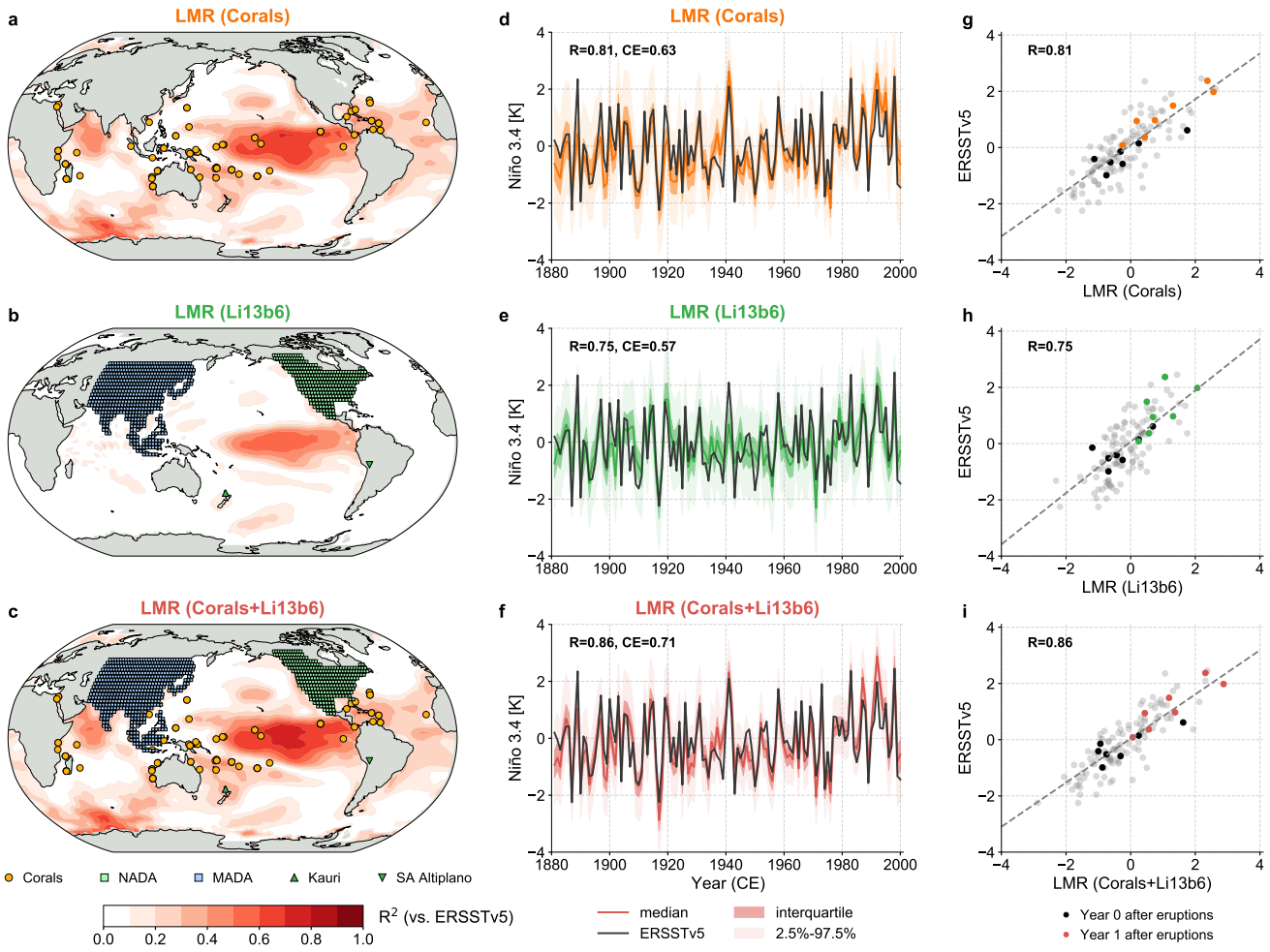

Fig. 1. (a-c) Spatial verification of the median field of the LMR[30,31] reconstructed boreal winter (December-February, DJF) surface temperature assimilating three sources: (a,d) corals from the Ocean2k compilation[29] updated with the latest Palmyra data[27]; (b,e) the six best predictors from Li et al.[10] (denoted as Li13b6), and (c,f) both data sources combined. Validation is performed against the Extended Reconstructed Sea Surface Temperature, Version 5 (ERSSTv5)[38] over the instrumental period (1881-2000 CE). The orange dots denote the location of the corals, the mint and blue squares denote the location of the North American Drought Atlas (NADA) (Version 2a)[39] and Monsoon Asia Drought Atlas (MADA)[40] sites, the green upward triangle denotes the location of the Kauri tree-ring composite[11], and the green downward triangle denotes the location of the South America Altiplano (SA Altiplano) tree-ring composite[42]. **(d-f)** Temporal verification of the median of the LMR reconstructed DJF Niño 3.4 series (colored curves) against the ERSSTv5 derived Niño 3.4 (black solid curve) over the instrumental period (1873-2000 CE). For each reconstruction, dark shading denotes the interquartile range, and light shading denotes the central 95% region, from 2.5% to 97.5%. R=correlation coefficient, CE=coefficient of efficiency[37]. **(g-i)** Scatter plot of the data points in (d-f). The grey dashed curve represents the linear regression fitting curve. The black and colored dots denote the data points at year 0 and year 1 relative to large eruption years (1883, 1902, 1913, 1951, 1963, 1982, 1991) as in Li et al.[10], respectively.

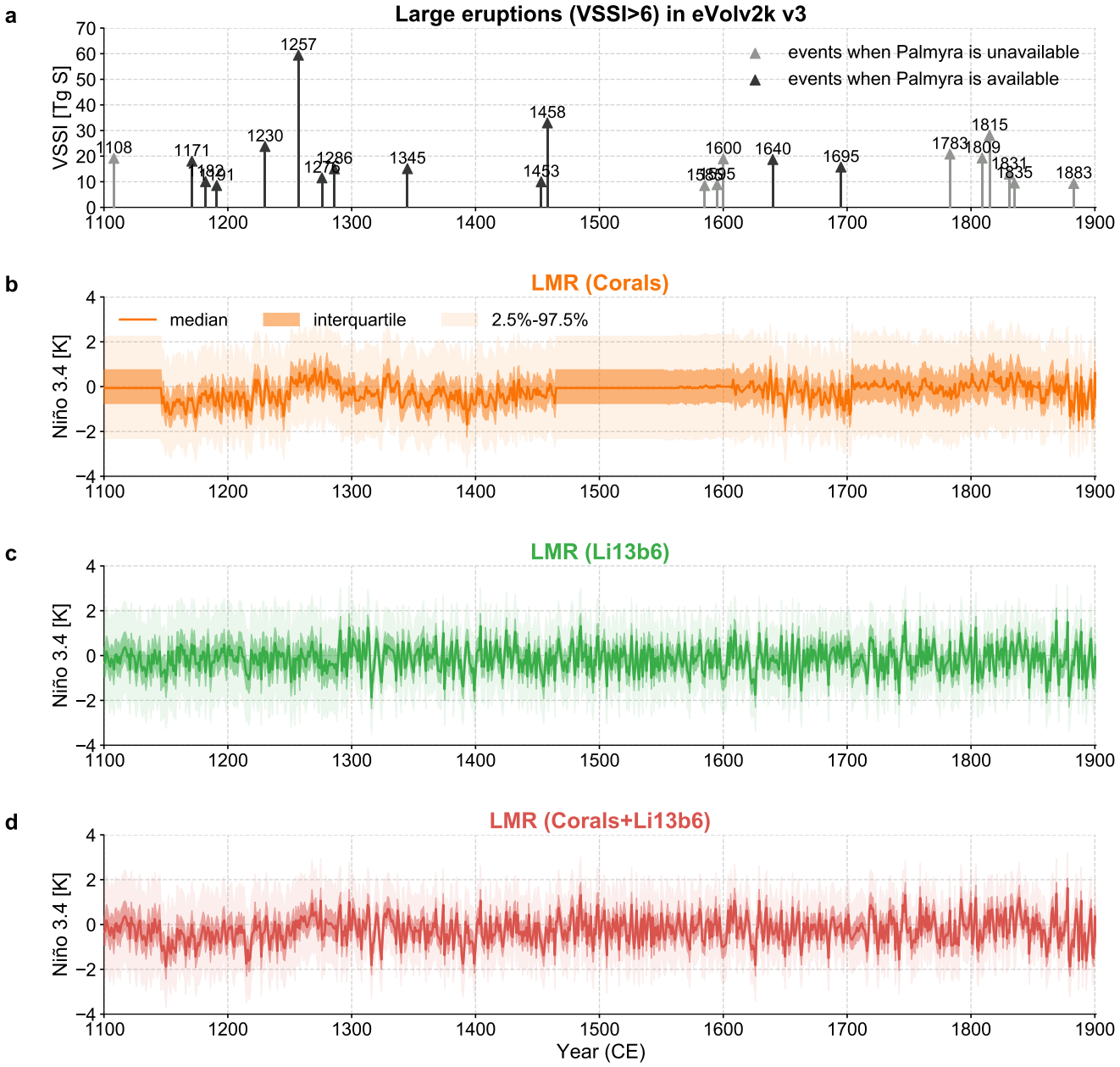

Fig. 2. **(a)** The 22 large eruption events defined as the volcanic stratospheric sulfur injection (VSSI) greater than 6 according to eVolv2k version 3[43]. 12 events over the years when the Palmyra coral record[26,27,35] is available are colored in black, while other events are colored in grey. See Extended Data Table 1 for the details of the metadata. **(b-d)** Same as Fig. 1d-f, but for the past millennium.

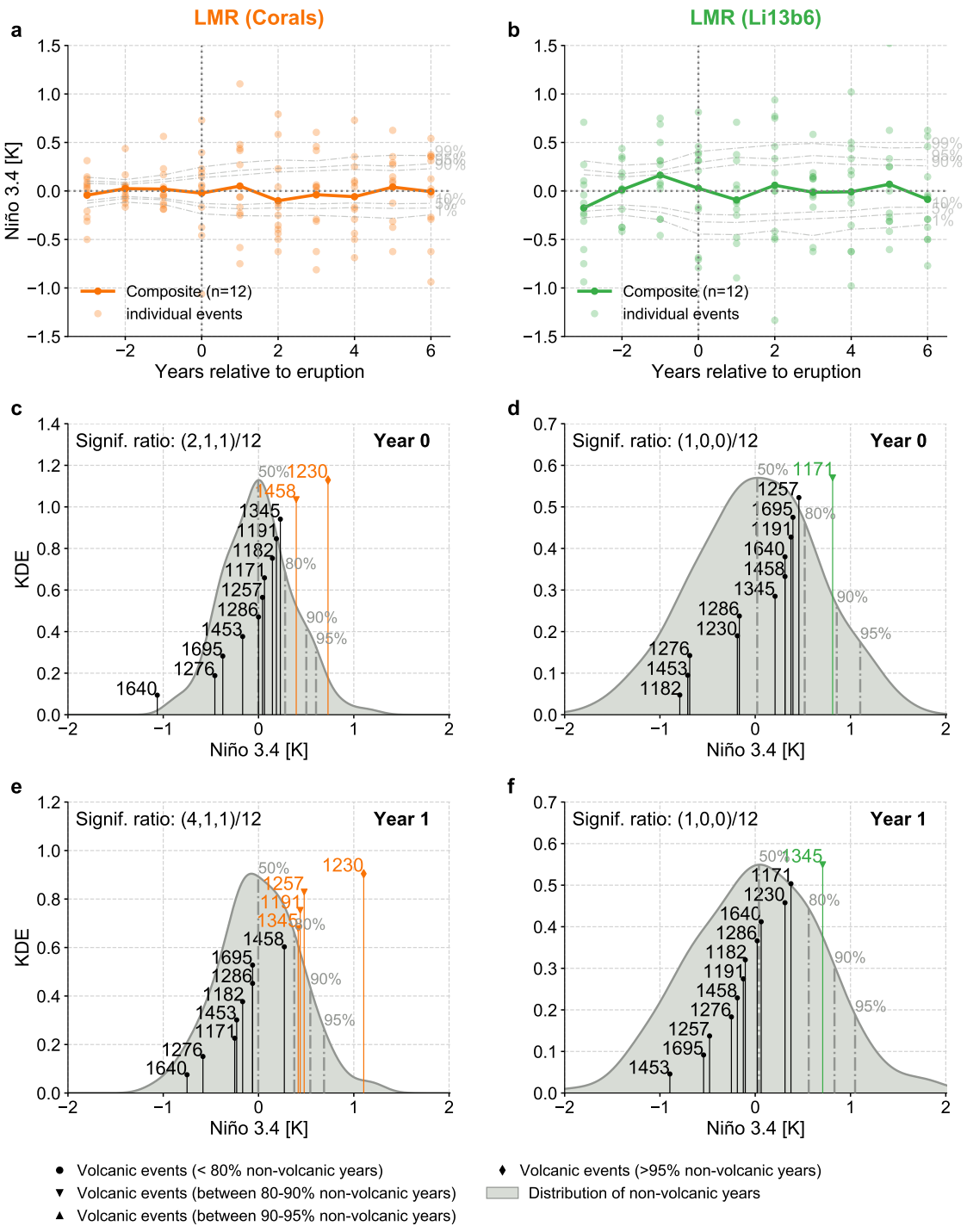

Fig. 3. (a-b) Superposed epoch analysis (SEA) of the reconstructions LMR (Corals) and LMR (Li13b6) regarding the 12 events when Palmyra is available. Solid curves with dots denote the composite mean, and the light dots denote the Niño 3.4 anomaly at each year for each individual event. The light grey dashed curves denote the 1%, 5%, 10%, 90%, 95%, and 99% quantiles of the composite means from 1000 bootstrap draws from non-volcanic years (Methods). **(c-d)** Ranking analysis of the LMR reconstructed Year 0 Niño 3.4 values. The grey shaded area denotes the distribution of the Niño 3.4 anomaly value over all non-volcanic years, whose 50%, 80%, 90%, and 95% quantiles are denoted by vertical dot-dashed curves, serving as significance levels (Methods). The vertical solid lines mark individual volcanic events; for each, the horizontal axis position denotes the Niño 3.4 anomaly value, and the vertical axis position denotes the relative rank of the Niño 3.4 anomaly value compared to all other events. The circle/downward triangle/upward triangle/diamond marker represents that a volcanic event has a Niño 3.4 anomaly value that is below 80%/between 80-90%/between 90-95%/above 95% of that over the non-volcanic years. The significance ratio denotes the number of events that are above the 80%, 90%, and 95% significance levels, respectively, out of all volcanic events. **(e-f)** Same as (c-d), but for the year 1 Niño 3.4 values.

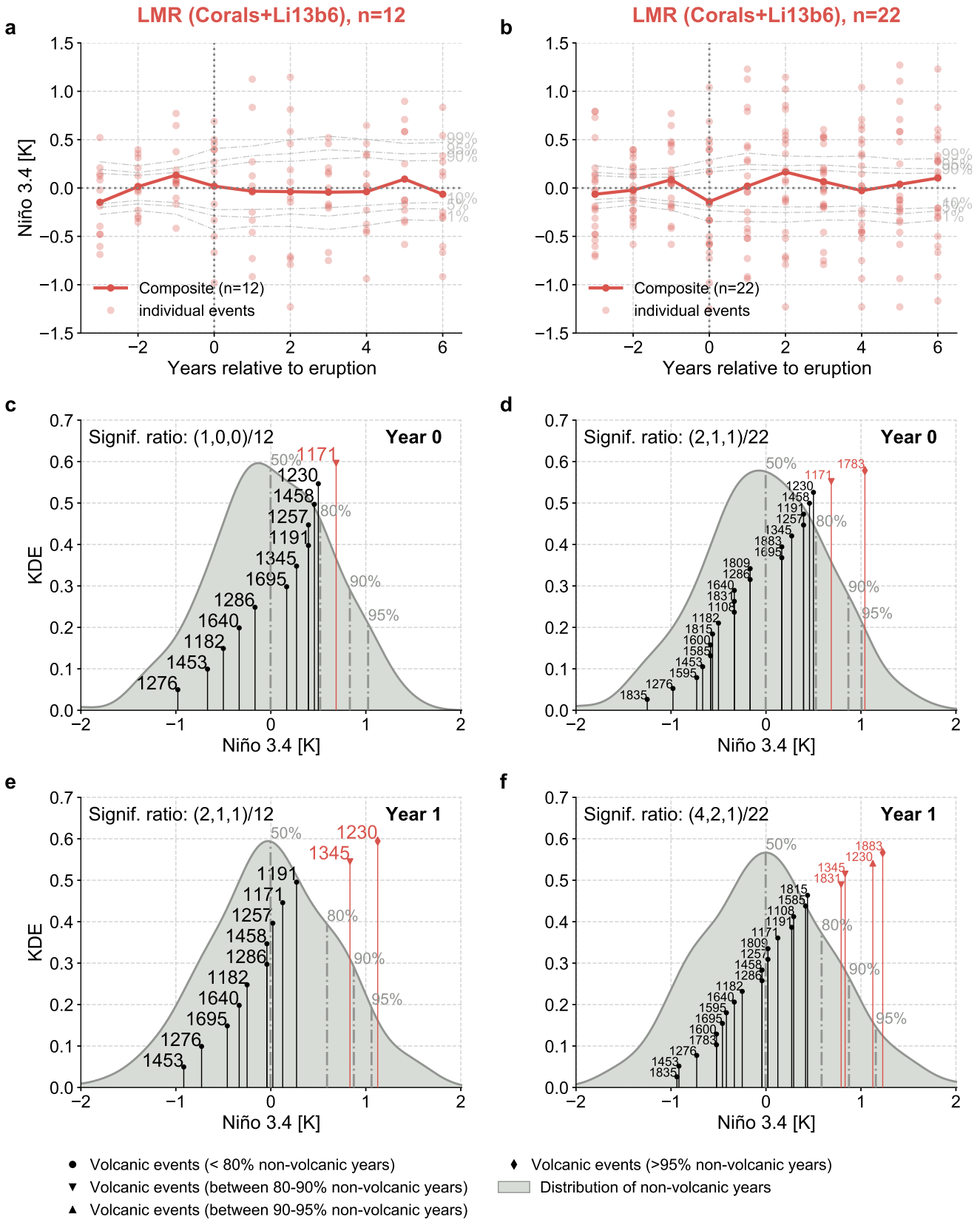

Fig. 4. Same as Fig. 3, but for LMR (Corals+Li13b6) regarding the 12 events when Palmyra is available and all the 22 events over the past millennium.

Extended Data Table 1. Metadata of the 22 large eruptions shown in Fig. 2a according to eVolv2k version 3[43]. Note that the value 0.0 in the column of Latitude denotes that the precise eruption latitude is unknown but the event is defined as tropical, and the value -1.0 in the column of Asymmetry (hemispheric asymmetry for tropical eruptions) denotes that the event is defined as extratropical.

Eruption year	Latitude	Asymmetry	VSSI
1108	0.0	4.0	19.16
1171	0.0	1.8	18.05
1182	45.0	-1.0	10.05
1191	0.0	0.7	8.53
1230	0.0	2.1	23.78
1257	-8.4	1.4	59.42
1276	0.0	0.2	11.53
1286	0.0	1.2	15.06
1345	0.0	1.4	15.11
1453	0.0	4.9	9.97
1458	0.0	0.6	32.98
1585	19.5	10.6	8.51
1595	4.9	0.8	8.87
1600	-16.6	2.0	18.95
1640	6.1	2.8	18.68
1695	0.0	1.1	15.74
1783	64.4	-1.0	20.81
1809	0.0	1.3	19.26
1815	-8.0	0.8	28.08
1831	19.5	8.1	12.98
1835	13.0	2.0	9.48
1883	-6.0	1.7	9.34

VSSI=volcanic stratospheric sulfur injection.

Asymmetry=hemispheric asymmetry (NH/SH) of aerosol spread for tropical eruptions based on ratio of Greenland to Antarctic flux.

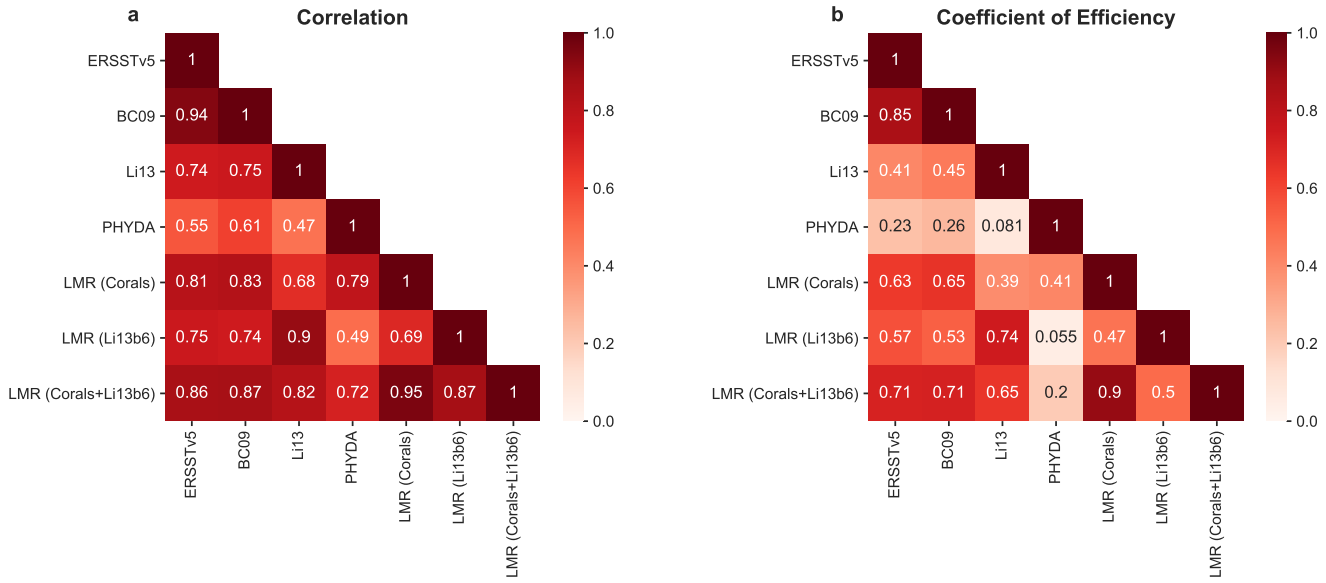

Extended Data Fig. 1. **(a)** Correlation coefficient and **(b)** coefficient of efficiency between instrumental observations and reconstructions of December-February (DJF) Niño 3.4 over timespan 1881-2000 CE. Data sources include: Extended Reconstructed Sea Surface Temperature, Version 5 (ERSSTv5)[38], Bunge and Clarke[66], Li et al.[10], the Paleo Hydrodynamics Data Assimilation product (PHYDA)[67], and the reconstructions of this study LMR (Corals), LMR (Li13b6), and LMR (Corals+Li13b6). Note that Li13 is a November-Januray (NDJ) reconstruction, and its correlation to NDJ ERSSTv5 and NDJ BC09 is 0.76 and 0.75, respectively, and the coefficient of efficient is 0.47 and 0.5, respectively.

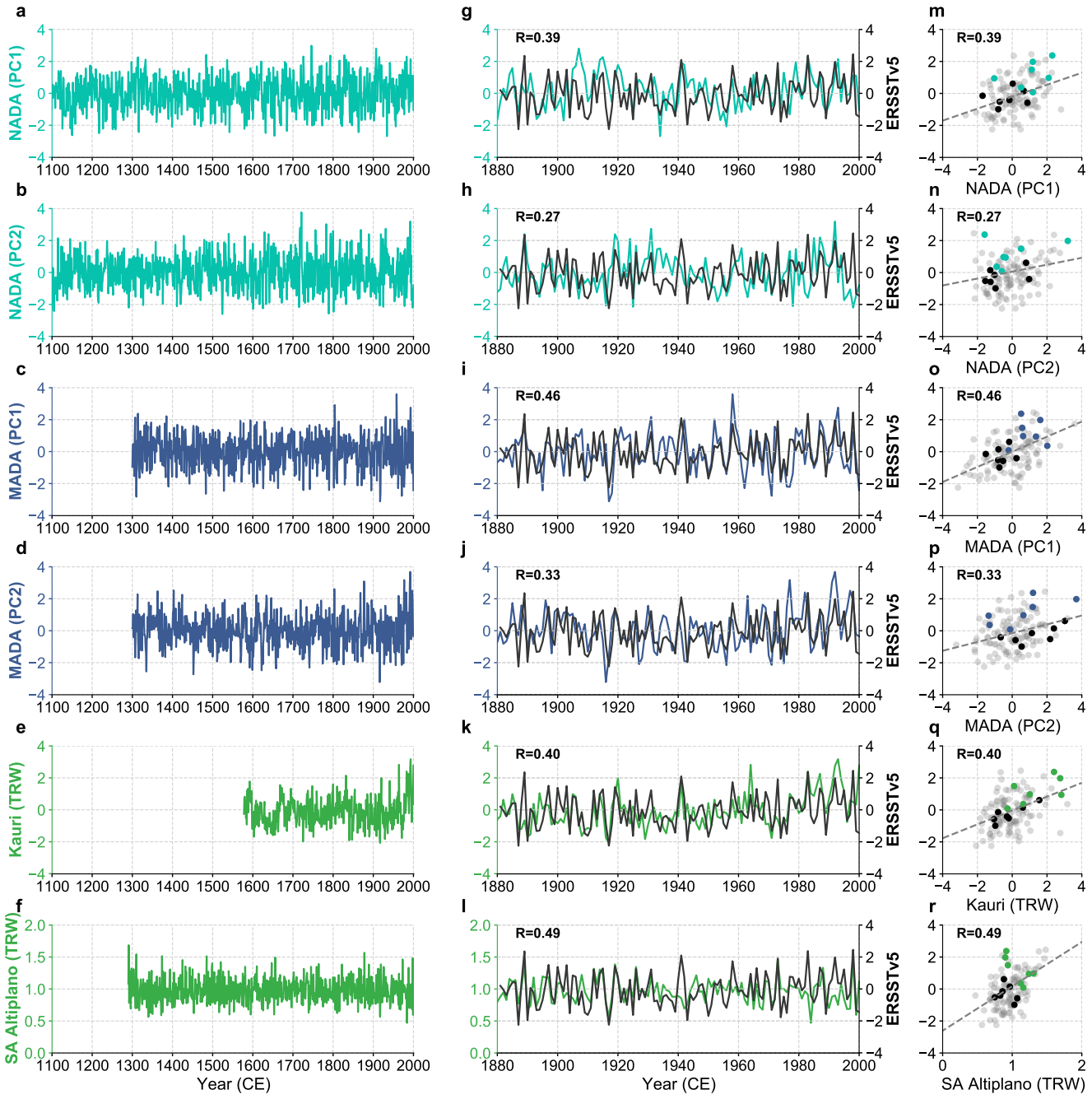

Extended Data Fig. 2. (a-f) Timeseries of the six best predictors from Li et al.[10], including the first two principle components of NADA and MADA, the Kauri tree-ring composite[41], as well as the South American Altiplano tree-ring composite[42], over the past millennium (1100-2000 CE). **(g-l)** Same as in (a-f), but over the instrumental period (1881-2000 CE). Validation is performed against the December-February (DJF) seasonally averaged Niño 3.4 calculated from Extended Reconstructed Sea Surface Temperature, Version 5 (ERSSTv5)[38] over the instrumental period (1881-2000 CE). **(m-r)** Scatter plots of the data points in (g-l). The black and colored dots denote the data points at year 0 and year 1 of large eruption years (1883, 1902, 1913, 1951, 1963, 1982, 1991) as in Li et al.[10], respectively. The dashed grey lines denote the linear regression fitting curves. R=correlation.

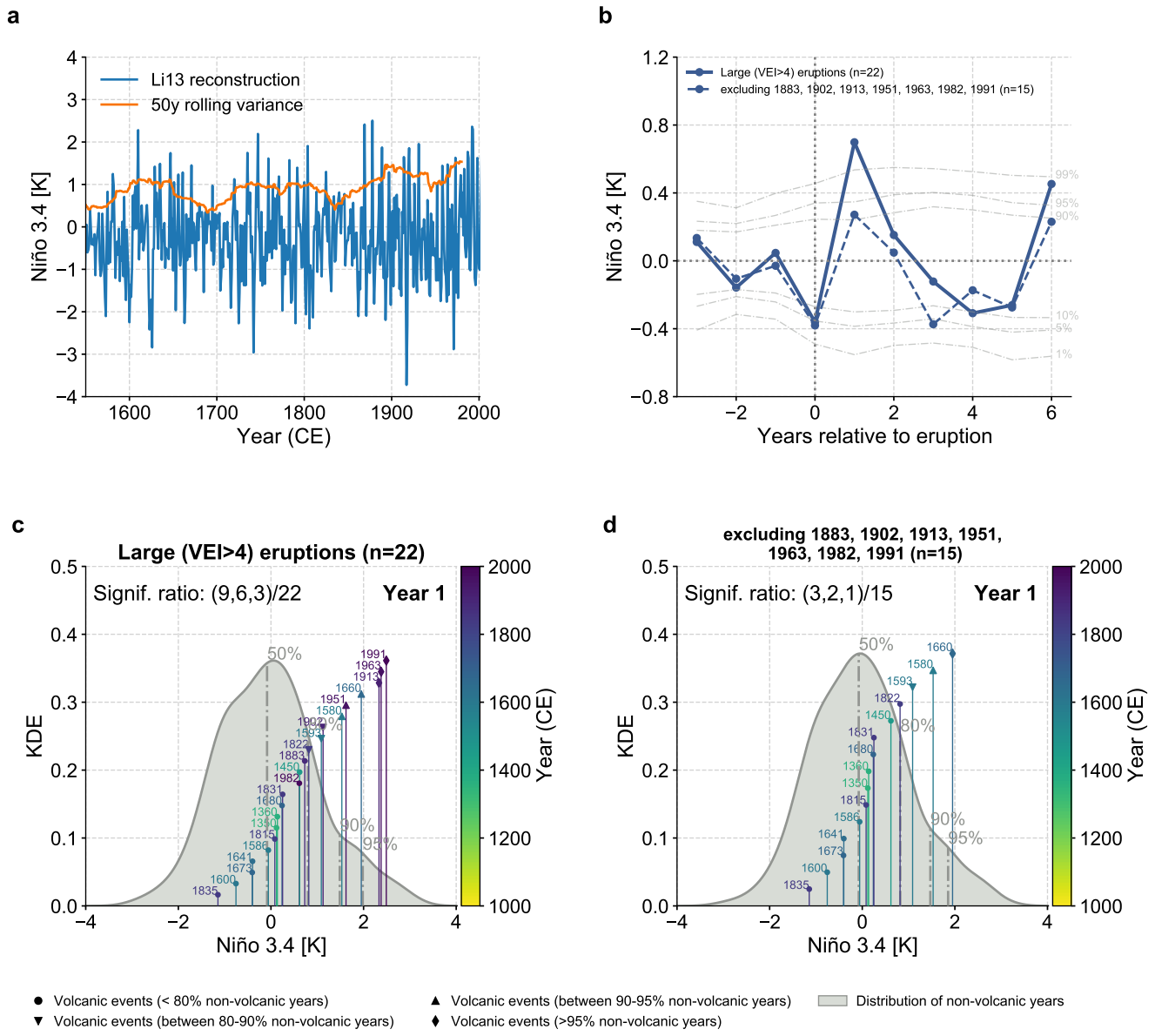

Extended Data Fig. 3. **(a)** The timeseries of the Li et al.[10] Niño 3.4 reconstruction (denoted as Li13). **(b)** SEA of Li13, comparing the pool of all 22 large eruptions defined as Volcanic Explosivity Index (VEI) larger than 4 and the pool excluding the events over the instrumental period after 1850 CE. **(c)** Ranking analysis of Li13 with the pool of all 22 large eruptions. **(d)** Ranking analysis of Li13 with the pool excluding the events over the instrumental period after 1850 CE. The color denotes the eruption year.

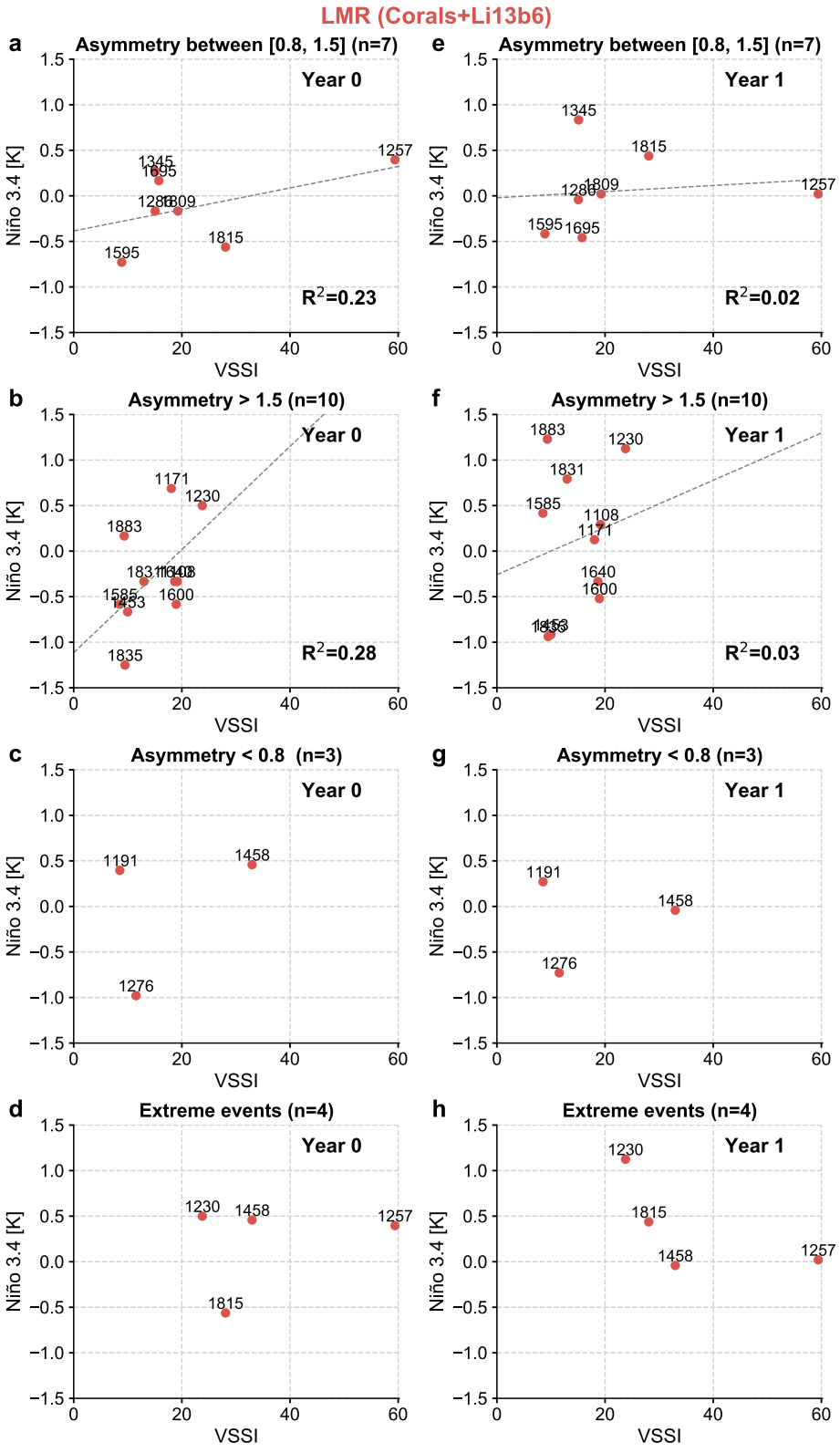

Extended Data Fig. 4. Scatter plots of the reconstructed year 0 and year 1 Niño 3.4 anomaly in LMR (Corals+Li13b6) against VSSI from eVolv2k version 3[43] for tropical eruption events listed in Extended Data Table 1, categorized by **(a, e)** Asymmetry between [0.8, 1.5], **(b, f)** Asymmetry > 1.5, **(c, g)** Asymmetry < 0.8 , as well as **(d, h)** extreme events with VSSI>20 (1230, 1257, 1458, 1815). The dashed grey lines denote the linear regression fitting curves. R=correlation coefficient. Asymmetry=hemispheric asymmetry (NH/SH) of aerosol spread for tropical eruptions based on ratio of Greenland to Antarctic flux.

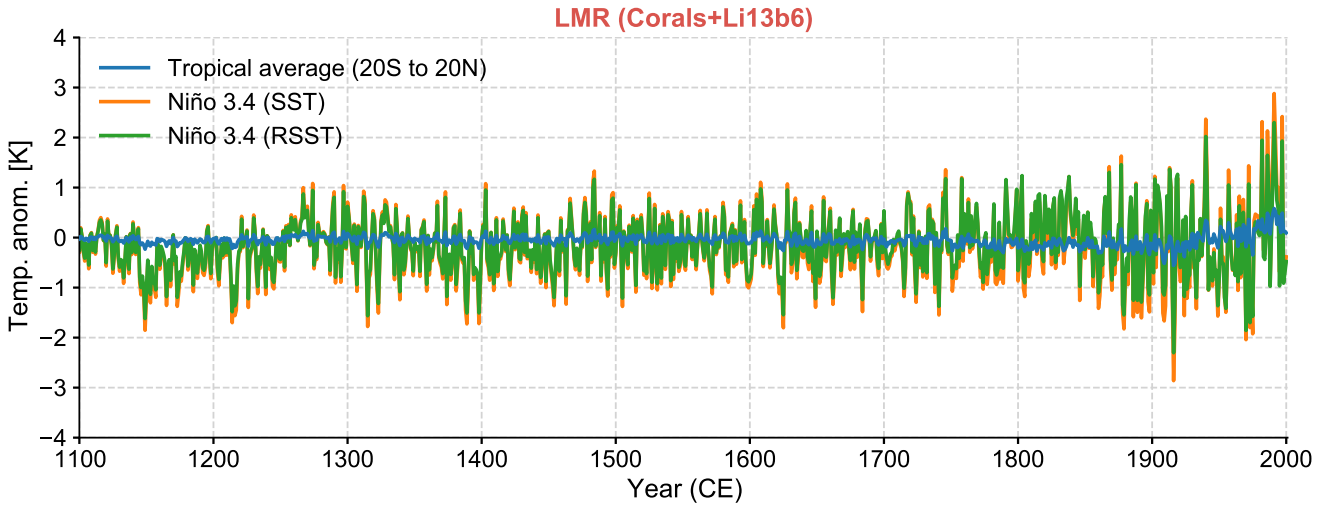

Extended Data Fig. 5. The timeseries of tropical average (20S-20N) temperature anomaly, sea surface temperature (SST) based Niño 3.4, and relative sea surface temperature (RSST)[17] based Niño 3.4.

Figures

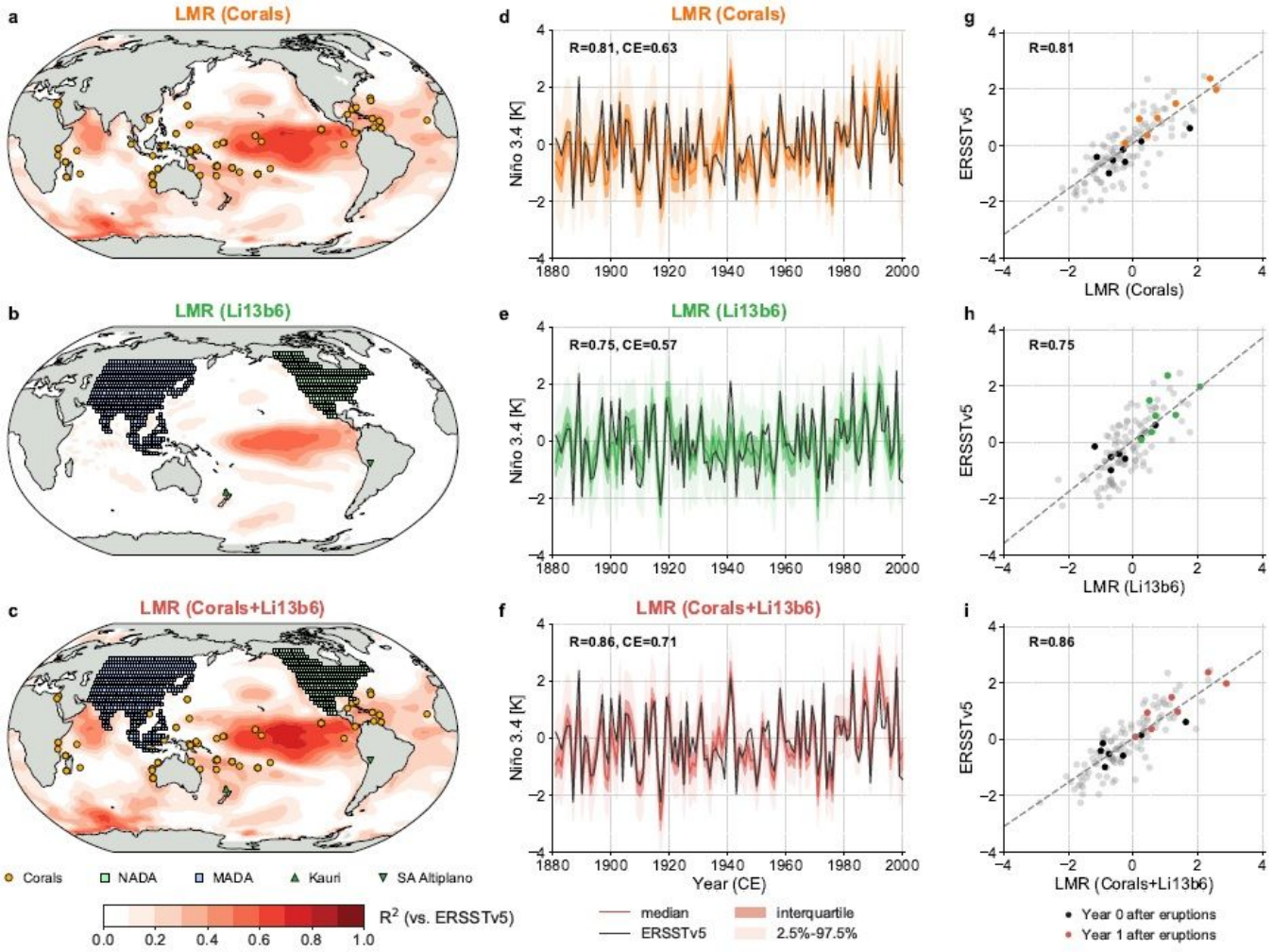

Figure 1

(a-c) Spatial verification of the median field of the LMR30, 31 reconstructed boreal winter (December-February, DJF) surface temperature assimilating three sources: (a,d) corals from the Ocean2k compilation29 updated with the latest Palmyra data27; (b,e) the six best predictors from Li et al.10 (denoted as Li13b6), and (c,f) both data sources combined. Validation is performed against the Extended Reconstructed Sea Surface Temperature, Version 5 (ERSSTv5)38 over the instrumental period (1881-2000 CE). The orange dots denote the location of the corals, the mint and blue squares denote the location of the North American Drought Atlas (NADA) (Version 2a)39 and Monsoon Asia Drought Atlas (MADA)40 sites, the green upward triangle denotes the location of the Kauri tree-ring composite11, and the green downward triangle denotes the location of the South America Altiplano (SA Altiplano) tree-ring composite42. (d-f) Temporal verification of the median of the LMR reconstructed DJF Niño 3.4 series (colored curves) against the ERSSTv5 derived Niño 3.4 (black solid curve) over the instrumental period (1873-2000 CE). For each reconstruction, dark shading denotes the interquartile range, and light shading denotes the central 95% region, from 2.5% to 97.5%. R=correlation coefficient, CE=coefficient of

efficiency37. (g-i) Scatter plot of the data points in (d-f). The grey dashed curve represents the linear regression fitting curve. The black and colored dots denote the data points at year 0 and year 1 relative to large eruption years (1883, 1902, 1913, 1951, 1963, 1982, 1991) as in Li et al.10, respectively. Note: The designations employed and the presentation of the material on this map do not imply the expression of any opinion whatsoever on the part of Research Square concerning the legal status of any country, territory, city or area or of its authorities, or concerning the delimitation of its frontiers or boundaries. This map has been provided by the authors.

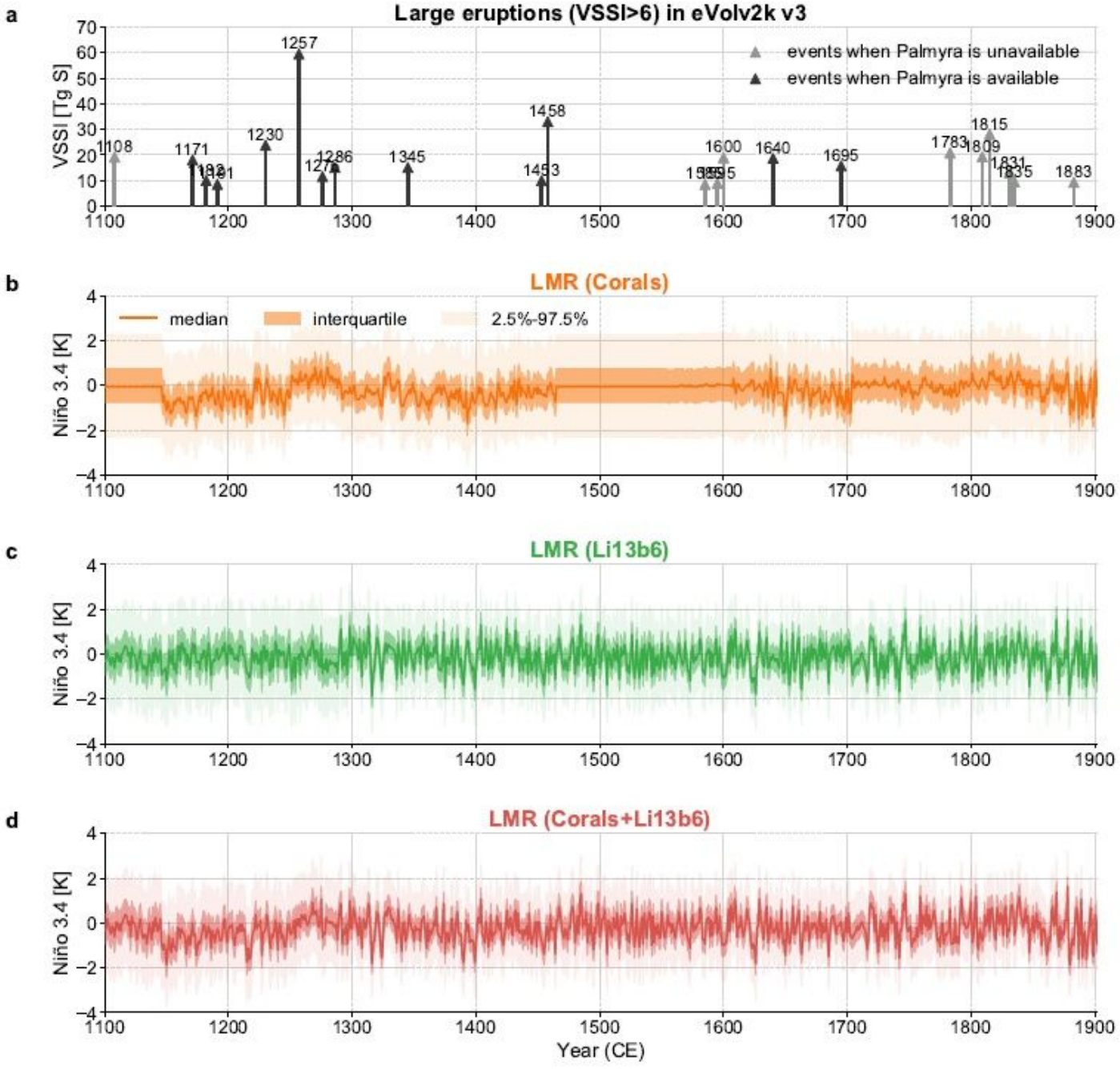

Figure 2

(a) The 22 large eruption events defined as the volcanic stratospheric sulfur injection (VSSI) greater than 6 according to eVolv2k version 343. 12 events over the years when the Palmyra coral record26, 27, 35 is available are colored in black, while other events are colored in grey. See Extended Data Table 1 for the details of the metadata. (b-d) Same as Fig. 1d-f, but for the past millennium.

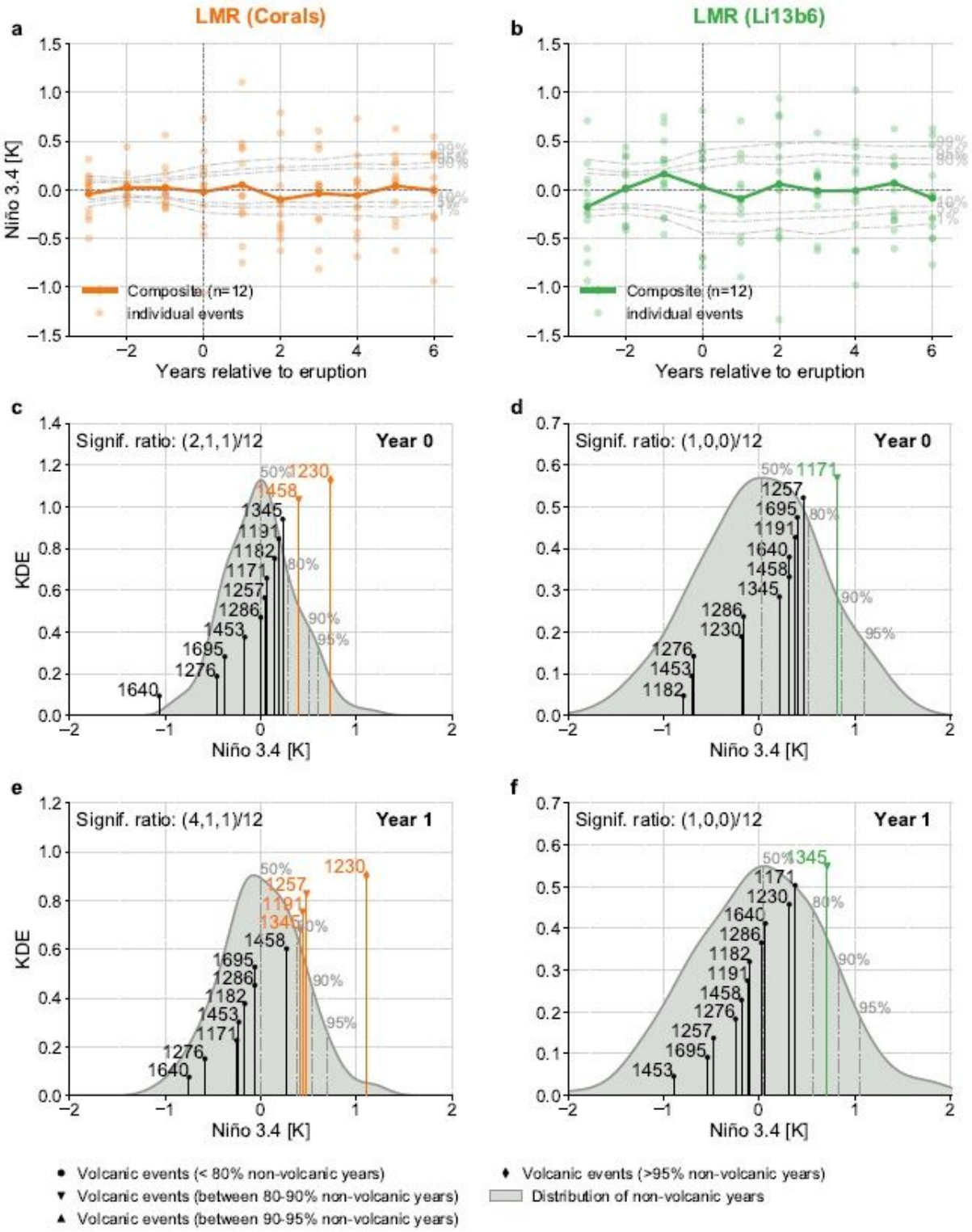

Figure 3

(a-b) Superposed epoch analysis (SEA) of the reconstructions LMR (Corals) and LMR (Li13b6) regarding the 12 events when Palmyra is available. Solid curves with dots denote the composite mean, and the light dots denote the Niño 3.4 anomaly at each year for each individual event. The light grey dashed curves denote the 1%, 5%, 10%, 90%, 95%, and 99% quantiles of the composite means from 1000 bootstrap draws from non-volcanic years (Methods). (c-d) Ranking analysis of the LMR reconstructed Year 0 Niño 3.4 values. The grey shaded area denotes the distribution of the Niño 3.4 anomaly value over all non-volcanic years, whose 50%, 80%, 90%, and 95% quantiles are denoted by vertical dot-dashed curves, serving as significance levels (Methods). The vertical solid lines mark individual volcanic events; for each, the horizontal axis position denotes the Niño 3.4 anomaly value, and the vertical axis position denotes the relative rank of the Niño 3.4 anomaly value compared to all other events. The circle/downward triangle/upward triangle/diamond marker represents that a volcanic event has a Niño 3.4 anomaly value that is below 80%/between 80-90%/between 90-95%/above 95% of that over the non-volcanic years. The significance ratio denotes the number of events that are above the 80%, 90%, and 95% significance levels, respectively, out of all volcanic events. (e-f) Same as (c-d), but for the year 1 Niño 3.4 values.

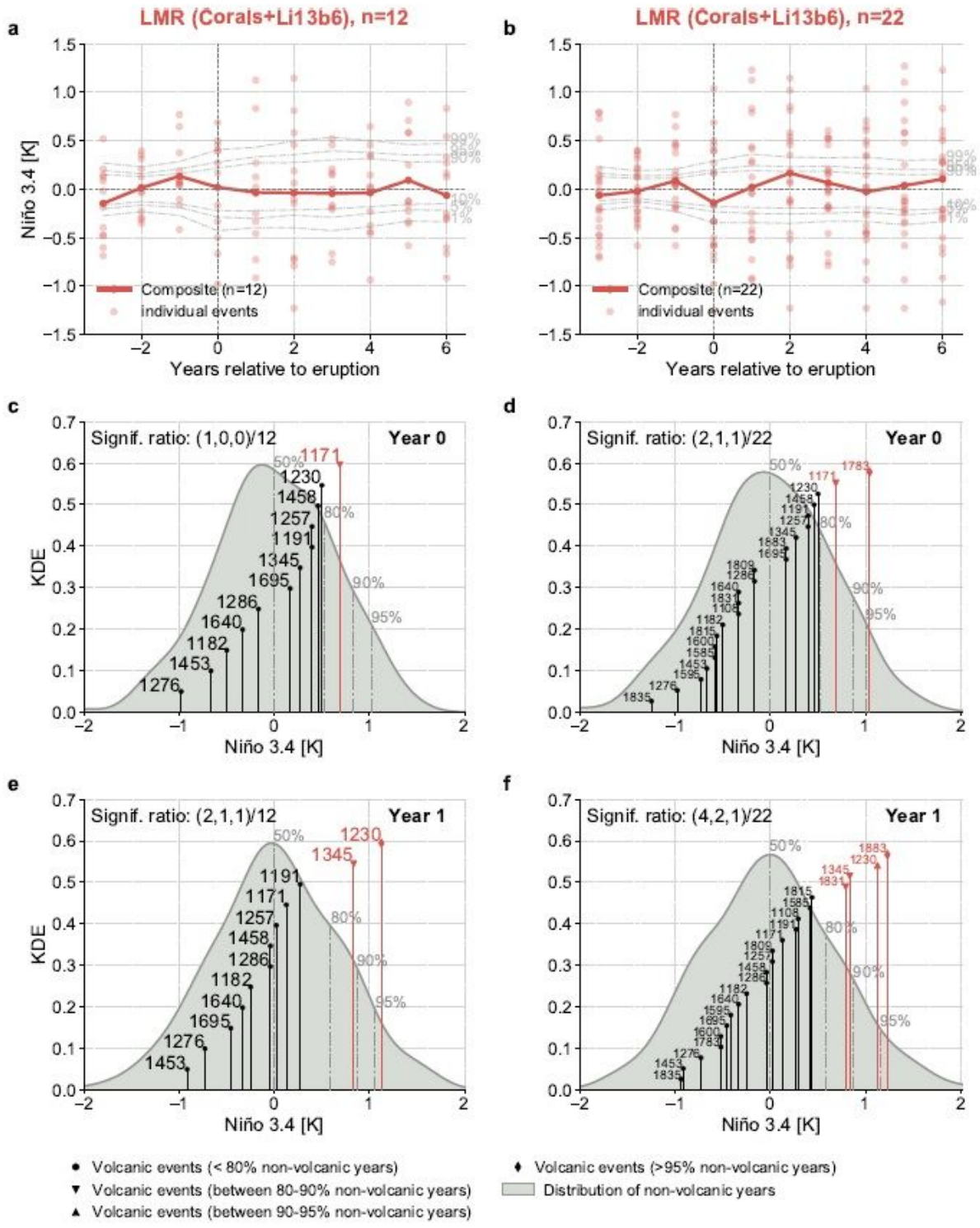

Figure 4

Same as Fig. 3, but for LMR (Corals+Li13b6) regarding the 12 events when Palmyra is available and all the 22 events over the past millennium.

Supplementary Files

This is a list of supplementary files associated with this preprint. Click to download.

- SI.pdf